PI3Kγ within a nonhematopoietic cell type negatively regulates diet-induced thermogenesis and promotes obesity and insulin resistance

Barbara Becattini[a,1], Romina Marone[b,1], Fabio Zani[a,1], Denis Arsenijevic[c], Josiane Seydoux[d], Jean-Pierre Montani[c], Abdul G. Dulloo[c], Bernard Thorens[e], Frédéric Preitner[e], Matthias P. Wymann[b,1,2], and Giovanni Solinas[a,1,2]

[a]Laboratory of Metabolic Stress Biology, Division of Physiology, Department of Medicine, University of Fribourg, CH-1700 Fribourg, Switzerland; [b]Cancer and Immunobiology Laboratory, Department of Biomedicine, Institute of Biochemistry & Genetics, CH-4058 Basel, Switzerland; [c]Division of Physiology, Department of Medicine, University of Fribourg, CH-1700 Fribourg, Switzerland; [d]Department of Basic Neurosciences, Faculty of Medicine, University of Geneva, CH-1211 Geneva, Switzerland; and [e]Mouse Metabolic Facility (MEF), Center for Integrative Genomics, University of Lausanne, CH-1015 Lausanne, Switzerland

Edited* by Michael Karin, University of California at San Diego School of Medicine, La Jolla, CA, and approved August 30, 2011 (received for review April 29, 2011)

Obesity is associated with a chronic low-grade inflammation, and specific antiinflammatory interventions may be beneficial for the treatment of type 2 diabetes and other obesity-related diseases. The lipid kinase PI3Kγ is a central proinflammatory signal transducer that plays a major role in leukocyte chemotaxis, mast cell degranulation, and endothelial cell activation. It was also reported that PI3Kγ activity within hematopoietic cells plays an important role in obesity-induced inflammation and insulin resistance. Here, we show that protection from insulin resistance, metabolic inflammation, and fatty liver in mice lacking functional PI3Kγ is largely consequent to their leaner phenotype. We also show that this phenotype is largely based on decreased fat gain, despite normal caloric intake, consequent to increased energy expenditure. Furthermore, our data show that PI3Kγ action on diet-induced obesity depends on PI3Kγ activity within a nonhematopoietic compartment, where it promotes energetic efficiency for fat mass gain. We also show that metabolic modulation by PI3Kγ depends on its lipid kinase activity and might involve kinase-independent signaling. Thus, PI3Kγ is an unexpected but promising drug target for the treatment of obesity and its complications.

energy balance | ectopic lipids | metabolic stress

Obesity is characterized by a chronic low-grade inflammation (1–5), and clinical studies suggest that antiinflammatory treatments may improve glucose homeostasis in diabetics (6–9). Thus, the identification of the molecular links between inflammation and metabolic homeostasis is fundamental to a better understanding of the pathophysiology of type 2 diabetes and other obesity-related diseases. Here, we have investigated the role of the lipid kinase PI3Kγ in diet-induced obesity, metabolic inflammation, and insulin resistance. PI3Kγ is the only class IB member of the PI3K family, and unlike the class IA PI3Ks (PI3Kα, PI3Kβ, and PI3Kδ), it was not implicated in insulin or insulin-like growth factor 1 (IGF-1) signaling (10–13). PI3Kγ is selectively recruited to G protein-coupled receptors implicated in inflammation and metabolic homeostasis, including chemokine receptors, β-adrenergic signaling, and angiotensin II receptors (13–17). On activation, PI3Kγ controls two major second messengers: phosphatidylinositol(3,4,5)-tris-phosphate (PIP_3) through direct phosphorylation of phosphatidylinositol 4,5 bisphosphate and cAMP by a kinase-independent mechanism (18). PI3Kγ is most abundant in cells of hematopoietic origin, but it is also expressed, at a much lower level, in a variety of nonhematopoietic cell types (19). Previous studies proposed a role for PI3Kγ in the control of insulin secretion, thereby suggesting that loss of PI3Kγ may predispose to glucose intolerance (20–22). By contrast, the results presented in this manuscript together with a recent study (23) show that mice lacking PI3Kγ are dramatically protected from diet-induced obesity and glucose intolerance. Kobayashi et al. (23) concluded that the improved glucose tolerance observed in mice lacking PI3Kγ is independent from their obesity-resistant phenotype. The latter study also proposes that PI3Kγ promotes insulin resistance mainly through a direct action within leukocytes to stimulate chemotaxis and consequent obesity-induced inflammation (23). However, here, we conclude that the obesity-resistant phenotype observed in mice lacking PI3Kγ is far from being negligible. Indeed, our results strongly suggest that obesity resistance is the main mechanism by which PI3Kγ inactivation protects from diet-induced inflammation and insulin resistance. We show that PI3Kγ activity within nonhematopoietic cells plays a major role in diet-induced obesity, hepatic steatosis, metabolic inflammation, and insulin resistance. Our data show that PI3Kγ-mediated metabolic modulation depends on a lipid kinase-dependent pathway, which promotes energetic efficiency for fat mass gain. Furthermore, we show that PI3Kγ lipid kinase-independent signaling negatively regulates hormone-sensitive lipase (HSL) activation within white adipose tissue.

Results

PI3Kγ Expression in White Adipose Tissue. We performed tissue distribution analysis of PI3Kγ mRNA levels by quantitative PCR (qPCR). As expected, PI3Kγ was highly expressed in bone marrow cells compared with other tissues, although we detected a relatively strong signal in white adipose tissue compared with other nonhematopoietic tissues (Fig. 1*A*). Furthermore, PI3Kγ mRNA levels were induced in adipose tissue of dietary and genetically obese mice (*ob*/*ob*) compared with lean animals (Fig. 1*A*). We have, therefore, compared PI3Kγ protein levels by immunoblot analysis in different white adipose tissue (WAT) pads, brown adipose tissue (BAT), and the heart, the latter being indicative of functional levels within nonhematopoietic cells (18). For all of the fat pads analyzed, we could detect a specific

Author contributions: M.P.W. and G.S. designed research; B.B., R.M., F.Z., D.A., J.S., F.P., and G.S. performed research; J.-P.M. and B.T. contributed new reagents/analytic tools; B.B., R.M., F.Z., D.A., J.S., A.G.D., F.P., M.P.W., and G.S. analyzed data; and B.B., R.M., M.P.W., and G.S. wrote the paper.

The authors declare no conflict of interest.

*This Direct Submission article had a prearranged editor.

Freely available online through the PNAS open access option.

[1]B.B., R.M., F.Z., M.P.W., and G.S. contributed equally to this work.

[2]To whom correspondence may be addressed. E-mail: Giovanni.Solinas@UniFr.CH or Matthias.Wymann@UniBas.CH.

See Author Summary on page 17251.

This article contains supporting information online at www.pnas.org/lookup/suppl/doi:10.1073/pnas.1106698108/-/DCSupplemental.

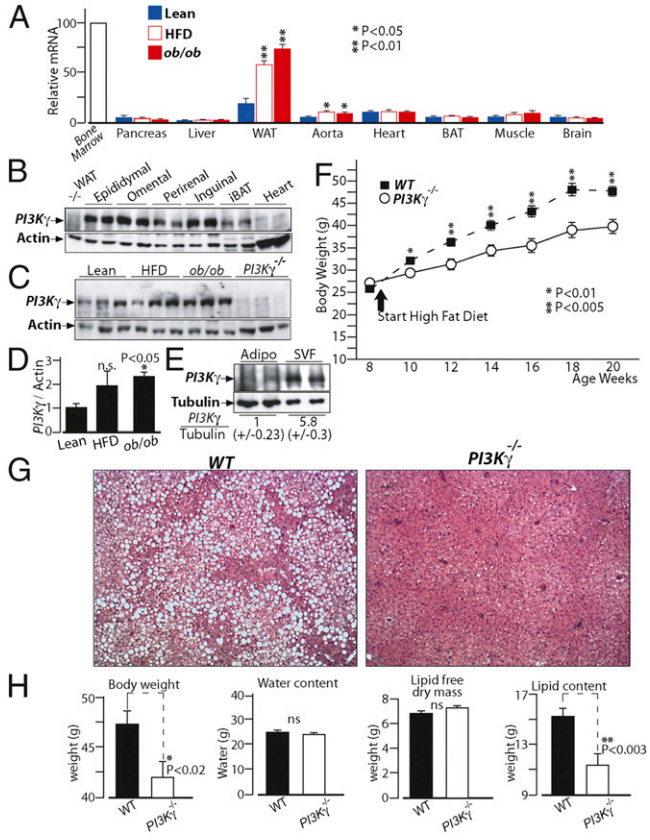

Fig. 1. PI3Kγ ablation in mice leads to dramatic protection from diet-induced obesity and fatty liver. (*A*) Real-time qPCR analysis of PI3Kγ mRNA levels in tissues from lean mice, diet-induced obese mice (HFD), and genetically obese mice (*ob/ob*). (*B*) Immunoblot analysis of PI3Kγ in different adipose tissue pads from WT mice kept on standard chow diet. Protein extracts from WAT of *PI3Kγ*$^{-/-}$ mice are loaded as control, and protein extracts from heart of WT mice are loaded for comparison. (*C*) Immunoblot analysis of PI3Kγ in epididymal adipose tissue of lean mice, HFD-induced obese mice, and *ob/ob* mice. (*D*) Densitometric quantification of the blots in *C*. (*E*) Immunoblot analysis of PI3Kγ in adipocytes and stromal vascular fractions (SVFs) of epididymal adipose tissue from diet-induced obese mice. (*F*) Growth curves of WT or *PI3Kγ*$^{-/-}$ mice placed on HFD. The beginning of HFD treatment is indicated. (*G*) H&E staining of liver sections from WT or *PI3Kγ*$^{-/-}$ mice placed on HFD. (*H*) Body composition of WT or *PI3Kγ*$^{-/-}$ mice placed on HFD.

band for PI3Kγ, whose intensity was much more pronounced than in the heart (Fig. 1*B*). Furthermore, PI3Kγ protein levels were increased in WAT of obese mice compared with lean ones (Fig. 1 *C* and *D*). PI3Kγ protein was more abundant in the stromal vascular fraction of WAT from obese mice, although it was also expressed in the mature adipocytes fraction (Fig. 1*E*).

Mice Lacking PI3Kγ Are Largely Protected from Diet-Induced Obesity and Hepatic Steatosis. To investigate the role of PI3Kγ in diet-induced obesity, WT C57BL6/J male mice or mice bearing a targeted gene mutation at the *PI3Kγ* locus (*PI3Kγ*$^{-/-}$) were placed either on standard chow diet or high-fat obesogenic diet (HFD) for 12 wk. On chow diet, *PI3Kγ*$^{-/-}$ mice and WT animals displayed comparable weight gains (Fig. S1*A* and S2 *A* and *D*) and similar body composition (Fig. S1 *B*–*E*). However, when placed on HFD, *PI3Kγ*$^{-/-}$ mice exhibited markedly reduced weight gain compared with WT mice (Fig. 1*F*). Such difference in body weight was independent from linear growth, whereas fat mass was decreased (Fig. S3). Liver, spleen, and kidney weights were also significantly reduced in *PI3Kγ*$^{-/-}$ mice compared with WT animals kept on HFD, possibly because of decreased ectopic lipids (Fig. S3). Indeed, histological analysis of liver sections revealed a dramatic protection from the development of fatty liver in *PI3Kγ*$^{-/-}$ mice compared with WT mice (Fig. 1*G*). Furthermore, body composition analysis showed that the weight gain difference between *PI3Kγ*$^{-/-}$ mice and WT mice is largely caused by total body lipids (adipose tissue and ectopic fat) (Fig. 1*H*).

Overall, *PI3Kγ*$^{-/-}$ mice are largely protected from diet-induced obesity and hepatic steatosis.

Mice Lacking *PI3Kγ* Display Markedly Improved Insulin Sensitivity That Correlates with Their Leaner Phenotype and Decreased Adipose Tissue Inflammation. To evaluate the impact of PI3Kγ inactivation on glucose homeostasis, we performed glucose tolerance test (GTT) and insulin tolerance test (ITT) in WT mice and *PI3Kγ*$^{-/-}$ mice placed either on chow diet or HFD. The growth curves of these mice are described in Fig. 1*F* and Fig. S1*A*. On chow diet, *PI3Kγ*$^{-/-}$ mice showed a significant improvement in insulin tolerance but similar glucose tolerance and skeletal muscle insulin signaling compared with WT mice at the age of 20 wk (Fig. S1). These results were recapitulated in a different cohort, where 6-mo-old *PI3Kγ*$^{-/-}$ mice on chow diet displayed improved insulin tolerance but comparable glucose tolerance with WT control animals (Fig. S2). Interestingly, at 1 y of age, *PI3Kγ*$^{-/-}$ mice showed better insulin and glucose tolerance than WT mice (Fig. S2). Most notably, we observed markedly improved insulin tolerance and glucose tolerance in *PI3Kγ*$^{-/-}$ mice compared with WT mice made obese by HFD (Fig. 2 *A* and *B*). To evaluate insulin sensitivity, we performed hyperinsulinemic euglycemic clamp. Radiolabeled 2-deoxy-D-glucose (2DOG) and glucose tracers were coinfused during the clamp to evaluate glucose uptake and glucose metabolism. *PI3Kγ*$^{-/-}$ mice displayed markedly improved systemic insulin sensitivity compared with WT mice kept on HFD. Indeed, *PI3Kγ*$^{-/-}$ mice showed about four times higher glucose infusion rate than WT mice (Fig. 2*C* and Fig. S4). This difference in systemic insulin sensitivity was because of an about two times higher glucose disposal rate and twofold better suppression of hepatic glucose production in *PI3Kγ*$^{-/-}$ mice compared with WT animals (Fig. 2 *D* and *E*). Consistently, 2DOG uptake was markedly elevated in gastrocnemius muscle during the clamp (Fig. 2*F*). A tendency for higher 2DOG uptake, although not significant ($P = 0.067$), was also observed in BAT from *PI3Kγ*$^{-/-}$ mice compared with control mice (Fig. 2*F*), whereas no difference was detected in epididymal WAT (Fig. S4*D*). Analysis of glucose metabolism during the clamp showed markedly enhanced glycolysis and glucose storage to glycogen and lipids in *PI3Kγ*$^{-/-}$ mice compared with WT mice (Fig. 2*G*). To learn about the contribution of the obesity-resistant phenotype observed in *PI3Kγ*$^{-/-}$ mice to their improved systemic insulin sensitivity, we have plotted the glucose infusion rate for each clamped mouse vs. its body weight. The results show a quasi-linear relationship between body weight and insulin resistance (Fig. 2*H*), which remarkably persisted even when glucose infusion rates were not normalized on body weight (Fig. 2*I*).

The improved insulin sensitivity observed in *PI3Kγ*$^{-/-}$ mice correlated with decreased adipose tissue inflammation (Fig. 2*J*). We observed a marked reduction of mRNA levels of the macrophage marker F4/80 and the mast cell marker FcεRI in WAT from *PI3Kγ*$^{-/-}$ mice compared with WT animals placed on HFD (Fig. 2*J*). Consistently, compared with WT controls, WAT from *PI3Kγ*$^{-/-}$ mice placed on HFD displayed reduced expression of chemotactic factors [monocyte chemotactic protein-1 (MCP-1), osteopontin, Chemokine (C-X-C motif) ligand 14 (CXCL14), and macrophage inflammatory protein 1 alpha (MIP-1α)] and proinflammatory mediators [plasminogen activator inhibitor-1 (PAI-1), TNFα, and IL-6]. An exception was IL-1β, whose expression was elevated to similar levels in WAT from *PI3Kγ*$^{-/-}$ mice and WT controls by the HFD treatment. Interestingly,

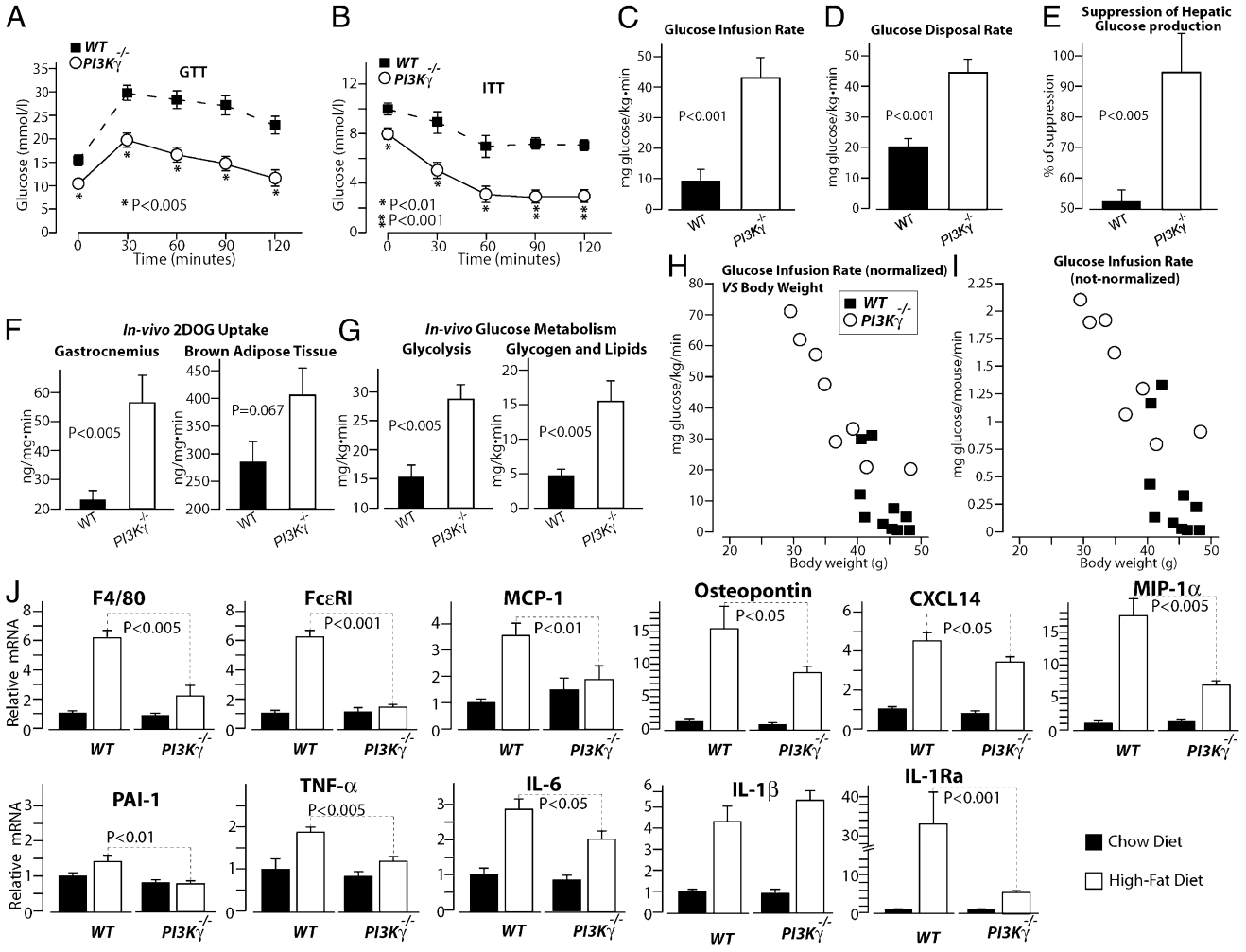

Fig. 2. *PI3Kγ*$^{-/-}$ mice placed on HFD display markedly improved glucose homeostasis, insulin sensitivity, and decreased adipose tissue inflammation. (*A*) GTT of WT and *PI3Kγ*$^{-/-}$ mice placed on HFD. (*B*) ITT of WT and *PI3Kγ*$^{-/-}$ mice on HFD. (*C–I*) Hyperinsulinemic euglycemic clamp analysis of WT and *PI3Kγ*$^{-/-}$ mice on HFD. (*C*) Glucose infusion rate. (*D*) Glucose disposal rate. (*E*) Percent of suppression of hepatic glucose production. (*F*) 2DOG uptake in gastrocnemius or BAT. (*G*) In vivo rate of glycolysis and storage of glucose to glycogen and lipids. (*H*) Glucose infusion rates from *C* are plotted for each clamped mouse vs. their body weights. Glucose infusion rates not normalized per body mass are plotted for each clamped mouse vs. their body weights. (*J*) Real-time qPCR analysis of mRNA levels of inflammatory markers in WAT from WT and *PI3Kγ*$^{-/-}$ mice placed on HFD.

IL-1Ra expression was largely reduced in WAT of *PI3Kγ*$^{-/-}$ mice relative to WT mice kept on HFD.

Overall, compared with WT controls, *PI3Kγ*$^{-/-}$ mice display marginally improved insulin tolerance but not glucose tolerance on standard chow diet up to the age of 6 mo; 1-y-old *PI3Kγ*$^{-/-}$ mice on chow diet showed a small but significant improvement in insulin and glucose tolerance compared with WT animals. On HFD, *PI3Kγ*$^{-/-}$ mice displayed largely improved glucose homeostasis because of improved systemic insulin sensitivity. Insulin resistance correlated with body weight, suggesting a major role for the lean phenotype of *PI3Kγ*$^{-/-}$ mice in their protection from HFD-induced insulin resistance. *PI3Kγ*$^{-/-}$ mice also displayed reduced WAT inflammation and markedly decreased IL-1Ra expression, despite similar IL-1β mRNA levels relative to WT mice.

Diet-Induced Obesity, Glucose Intolerance, and Inflammation Depend on PI3Kγ Activity Within a Nonhematopoietic Compartment. To learn about the mechanism of PI3Kγ in diet-induced obesity, insulin resistance, and metabolic inflammation, we investigated the metabolic action of PI3Kγ specifically in hematopoietic and nonhematopoietic cells by bone marrow transplantation experiments (24). WT and *PI3Kγ*$^{-/-}$ mice were lethally irradiated, and their hematopoietic cells were reconstituted with bone marrow cells either from WT or *PI3Kγ*$^{-/-}$ mice to generate the following mice: a control group *WT* + *WT-BM*, where WT recipient mice were reconstituted with bone marrow cells from WT donor mice; *WT* + *PI3Kγ*$^{-/-}$*-BM*, where WT mice were reconstituted with *PI3Kγ*$^{-/-}$ bone marrow (hematopoietic-specific *PI3Kγ* KO); *PI3Kγ*$^{-/-}$ + *WT-BM*, where *PI3Kγ*$^{-/-}$ mice were reconstituted with WT bone marrow (nonhematopoietic-specific *PI3Kγ* KO); and *PI3Kγ*$^{-/-}$+ *PI3Kγ*$^{-/-}$*-BM*, where *PI3Kγ*$^{-/-}$ mice were reconstituted with *PI3Kγ*$^{-/-}$ bone marrow (Fig. 3*A*). Flow cytometry analysis shows that white blood cells, peripheral blood monocytes (CD11b-positive cells), and lymphocytes (CD3-positive cells) were efficiently reconstituted (Fig. S5*A*). Furthermore, peritoneal mast cells (FcεRI/cKit double positive cells) were also efficiently reconstituted (Fig. S5*A*). Immunoblot analysis revealed that, in WAT, PI3Kγ is mainly expressed within hematopoietic cells (Fig. S5 *G* and *I*). By contrast, growth curves showed that the obesity-resistant phenotype of *PI3Kγ*$^{-/-}$ mice is caused by a radiation-resistant cell type of nonhematopoietic origin. Indeed, *WT* + *PI3Kγ*$^{-/-}$*-BM* chimeras displayed a similar weight gain to *WT* + *WT-BM* control mice, whereas *PI3Kγ*$^{-/-}$ + *WT-BM* mice

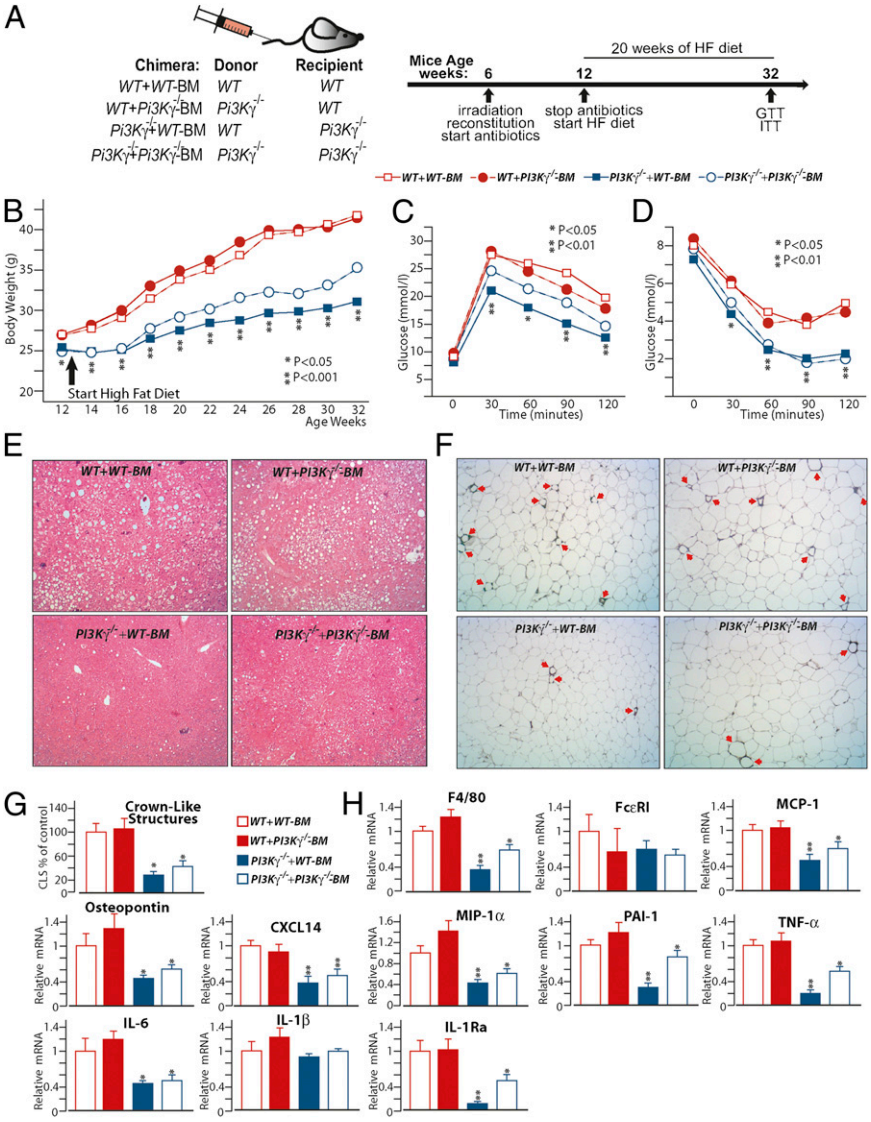

Fig. 3. PI3Kγ-mediated metabolic modulation operates within a nonhematopoietic compartment. (*A*) List of the radiation chimeras generated and experimental design. (*B*) Growth curves of the different radiation chimeras kept on HFD. (*C*) GTT of the radiation chimeric mice on HFD. (*D*) Insulin tolerance of the radiation chimeras on HFD. (*E*) H&E staining of liver sections from the different radiation chimeras on HFD. (*F*) MAC2 staining of WAT sections from the above-described chimeras, and (*G*) quantification of crown-like structures from *F* expressed as percentage of controls (*WT* + *WT-BM*). (*H*) Real-time qPCR analysis of mRNA levels of inflammatory markers in WATs from the different radiation chimeras placed on HFD. *P* values in *B–D* are for comparisons between *WT* + *WT-BM* and *PI3Kγ*$^{-/-}$ + *WT-BM*.

were markedly obesity-resistant (Fig. 3*B*). Inactivation of PI3Kγ in both hematopoietic and nonhematopoietic compartments (*PI3Kγ*$^{-/-}$ + *PI3Kγ*$^{-/-}$*-BM*) did not further exacerbate the leaner phenotype observed in the nonhematopoietic-specific *PI3Kγ*$^{-/-}$ + *WT-BM* group (Fig. 3*B*). Fed insulin serum levels were also specifically decreased by PI3Kγ ablation within nonhematopoietic cells (Fig. S5 *B* and *C*). Improved glucose homeostasis was also because of the nonhematopoietic compartment. Indeed, *WT* + *PI3Kγ*$^{-/-}$*-BM* mice and *WT* + *WT-BM* control mice displayed similar glucose and insulin tolerance, whereas *PI3Kγ*$^{-/-}$ + *WT-BM* mice showed largely improved glucose and insulin tolerance compared with *WT* + *WT-BM* controls (Fig. 3 *C* and *D* and Fig. S5 *D* and *E*). *PI3Kγ*$^{-/-}$ + *PI3Kγ*$^{-/-}$*-BM* mice did not show additional improvement in glucose and insulin tolerance compared with the nonhematopoietic-specific *PI3Kγ*$^{-/-}$ + *WT-BM* mice (Fig. 3 *C* and *D* and Fig. S5 *D* and *E*). Furthermore, *WT* + *WT-BM* control mice and *WT* + *PI3Kγ*$^{-/-}$*-BM* chimeras developed steatosis to a similar degree, whereas *PI3Kγ*$^{-/-}$ + *WT-BM* and *PI3Kγ*$^{-/-}$ + *PI3Kγ*$^{-/-}$*-BM* mice were largely protected (Fig. 3*E*). Finally, mice lacking PI3Kγ in hematopoietic cells only (*WT* + *PI3Kγ*$^{-/-}$*-BM*) displayed similar WAT inflammatory gene expression profile and crown-like structure number to *WT* + *WT-BM* mice (Fig. 3 *F–H*). By contrast, *PI3Kγ*$^{-/-}$ + *WT-BM* mice displayed fewer crown-like structures, decreased expression of the macrophage marker F4/80, and chemokines (MCP-1, osteopontin, and CXCL14) (Fig. 3 *F–H*). The adipokines PAI-1, TNFα, IL-6, and IL-1βRa, but not IL-1β, were also decreased in WAT from *PI3Kγ*$^{-/-}$ + *WT-BM* mice compared with *WT* + *WT-BM* mice (Fig. 3*H*). PI3Kγ inactivation in both hematopoietic and nonhematopoietic cells (*PI3Kγ*$^{-/-}$ + *PI3Kγ*$^{-/-}$*-BM*) did not further reduce adipose tissue inflammation (Fig. 3 *F–H*). Interestingly, WAT inflammation correlated with the number of hypertophic adipocytes, which were specifically reduced in mice lacking *PI3Kγ* within the nonhematopoietic compartment (Fig. S5*F*).

Altogether, our results show that hematopoietic cells are the major expression site for PI3Kγ within WAT, but resistance to diet-induced obesity and hepatic steatosis improved insulin sensitivity; additionally, the decreased WAT inflammation observed in *PI3Kγ*$^{-/-}$ mice was mainly because of a radiation-resistant cell type of nonhematopoietic origin.

Mice Lacking PI3Kγ Display Reduced Weight Gain Efficiency on HFD and Exacerbated HFD-Induced Thermogenesis. To further investigate the mechanism of *PI3Kγ*$^{-/-}$ mice obesity-resistant phenotype, we performed an energy balance of the weight gain of the mice on HFD. Food intake was measured for 6 wk in special cages designed to avoid food spillage (for maximal precision and sensitivity), and we recorded body weights during the food intake measurements. Fecal lipid content was also measured to investigate eventual defects in intestinal lipid absorption. During the food intake measurements, *PI3Kγ*$^{-/-}$ mice displayed markedly reduced weight gain on HFD compared with WT mice, despite similar food intake (Fig. 4 *A–F*). Thereby, *PI3Kγ*$^{-/-}$ mice show a reduced efficiency for body mass gain per consumed food relative to WT animals (Fig. 4 *G* and *H*). This observation motivated us to investigate the role of PI3Kγ in the adaptive thermogenesis to HFD feeding. *PI3Kγ*$^{-/-}$ and WT mice were placed into an indirect calorimeter for 3 d on chow diet (when they had similar body weight and composition), and then, the animals were kept on HFD for 3 more d. Mice adapted to the new environment during the first 2 d, and thus, data were collected from day 3 of chow diet. At the end of the third day of chow diet, the mice were switched to HFD in the calorimeter, and data were collected for 60 h. Consistent with previous reports (25), WT mice showed increased oxygen consumption per kilogram of body weight in response to HFD (Fig. 4 *I* and *J*). *PI3Kγ*$^{-/-}$ mice displayed higher oxygen consumption per body mass compared with WT mice, which reached statistical significance on the second light period and third dark period on HFD (Fig. 4*I*). To investigate the role of PI3Kγ in the thermogenic response to HFD, we calculated the increase in caloric expenditure per mouse caused by HFD. The results show that the thermogenic response to HFD per mouse was significantly higher for *PI3Kγ*$^{-/-}$ mice compared with WT mice after 3 d on HFD (Fig. 4*J*). *PI3Kγ*$^{-/-}$ mice displayed increased physical activity compared with WT mice during the calorimetry, but differences in physical activity did not correlate with differences in energy expenditure (Fig. S6).

Metabolic Phenotype of *PI3Kγ*$^{-/-}$ Mice Is Qualitatively Conserved at Thermoneutrality. *PI3Kγ*$^{-/-}$ mice placed on HFD display decreased energetic efficiency for lipid deposition and increased HFD-induced thermogenesis compared with WT control animals (Fig. 4). Thus, the difference in energy balance observed between WT and *PI3Kγ*$^{-/-}$ mice kept on HFD is most likely caused by an energy expenditure mechanism, such as adaptive thermogenesis (26). A major factor controlling adaptive thermogenesis is environmental temperature (26). To investigate the contribution of thermoregulatory thermogenesis to the metabolic phenotype of *PI3Kγ*$^{-/-}$ mice, we placed *PI3Kγ*$^{-/-}$ mice and WT controls on HFD at thermoneutrality (30 °C), where the energetic cost for body temperature maintenance is minimal. *PI3Kγ*$^{-/-}$ mice kept on HFD at 30 °C gained less weight compared with WT animals (Fig. 5*A*), although this difference was less pronounced than genotypic differences observed at room temperature (Fig. 1*F*). Relative to WT mice, *PI3Kγ*$^{-/-}$ mice also displayed a partial protection from hepatic steatosis (Fig. 5*B*) and improved glucose and insulin tolerance (Fig. 5 *C* and *D*). Consistently, WAT gene expression profiling showed reduced mRNA levels of F4/80, FcεRI, MCP-1, osteopontin, MIP-1α, PAI-1, TNF-α, IL-6, and IL-1Ra in *PI3Kγ*$^{-/-}$ mice compared with WT mice, whereas IL-1β and CXCL14 mRNA levels were unchanged (Fig. 5*E*).

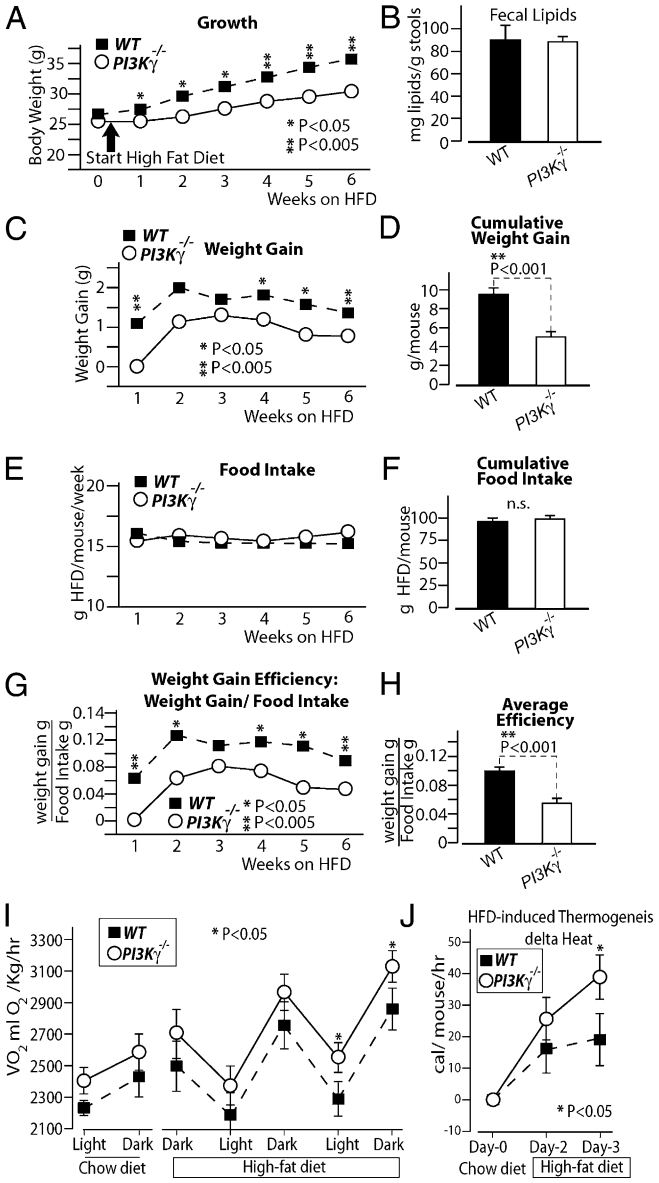

Fig. 4. Loss of PI3Kγ reduces weight gain efficiency on HFD and promotes adaptive thermogensis to HFD. (*A–H*) Energy balance study of WT or *PI3Kγ*$^{-/-}$ mice placed on HFD for 6-wk: (*A*) growth curve, (*B*) fecal lipid content, (*C*) weekly weight gains, (*D*) 6-wk cumulative weight gain, (*E*) weekly food intakes, (*F*) 6-wk cumulative food intake, (*G*) weight gain efficiency (expressed as gained weight per food intake), and (*H*) average weight gain efficiency over 6 wk. (*I* and *J*) Indirect calorimetric analysis of WT and *PI3Kγ*$^{-/-}$ mice during the transition from chow to HFD.

Altogether, our results show that the metabolic phenotype of *PI3Kγ*$^{-/-}$ mice is qualitatively reproduced at thermoneutrality, but they also indicate that this phenotype is likely enhanced by thermoregulatory thermogenesis at room temperature.

Selective Loss of PI3Kγ Kinase Activity Recapitulates the Metabolic Phenotype of *PI3Kγ*$^{-/-}$ Mice. PI3Kγ signals through a lipid kinase-dependent pathway to generate PIP_3 and a kinase-independent pathway that negatively regulates cAMP levels (18). To evaluate the specific contribution of the kinase-dependent pathway to the phenotype observed in *PI3Kγ*$^{-/-}$ mice, we investigated mice expressing a kinase-dead mutant of PI3Kγ (*PI3Kγ*$^{KD/KD}$). *PI3Kγ*$^{KD/KD}$ mice have no PI3Kγ kinase activity but retain PI3Kγ kinase-independent action on cAMP (18). On standard chow

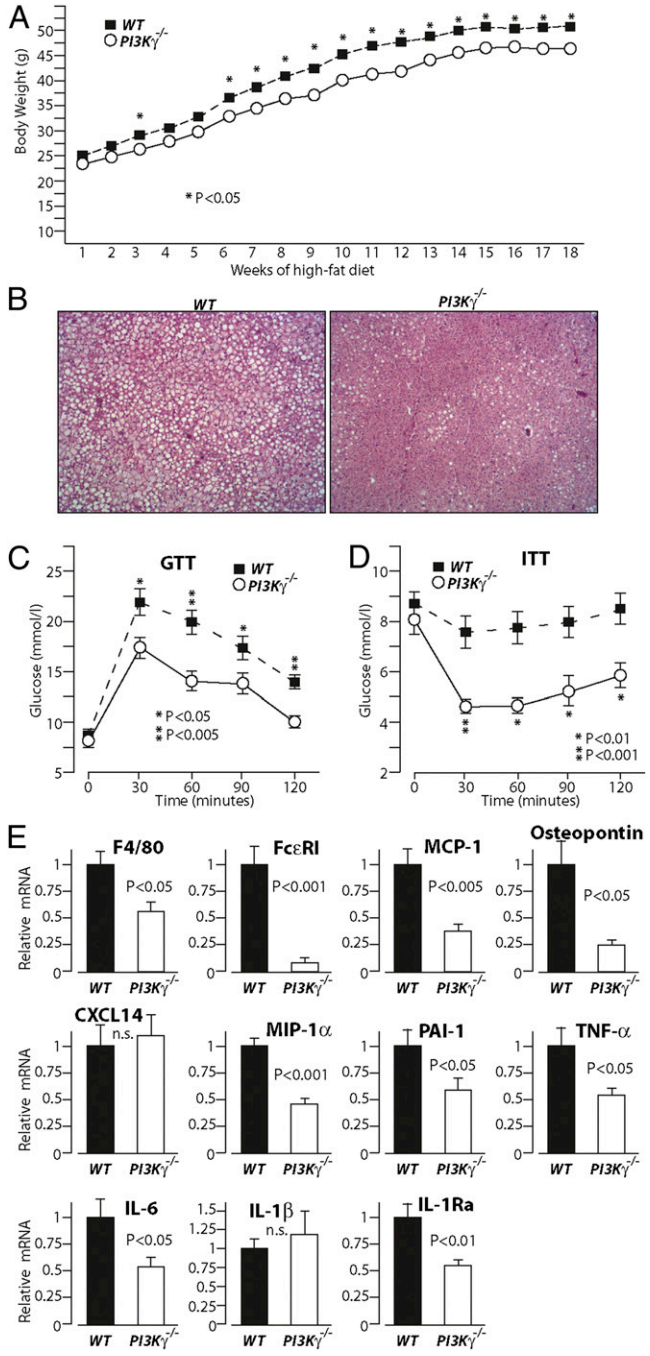

Fig. 5. The metabolic phenotype of *PI3Kγ*$^{-/-}$ mice is qualitatively conserved at thermoneutrality. (*A*) Growth curves of WT or *PI3Kγ*$^{-/-}$ mice placed on HFD in a thermoneutral environment (30 °C). (*B*) H&E staining of liver sections from WT or *PI3Kγ*$^{-/-}$ mice on HFD at 30 °C. (*C*) GTT of WT and *PI3Kγ*$^{-/-}$ mice on HFD at 30 °C. (*D*) ITT of WT and *PI3Kγ*$^{-/-}$ mice on HFD at 30 °C. (*E*) qPCR analysis of mRNA levels of inflammatory markers in epididimal adipose tissue from WT and *PI3Kγ*$^{-/-}$ mice kept on HFD at 30 °C. Mice were 8 wk old when placed on HFD.

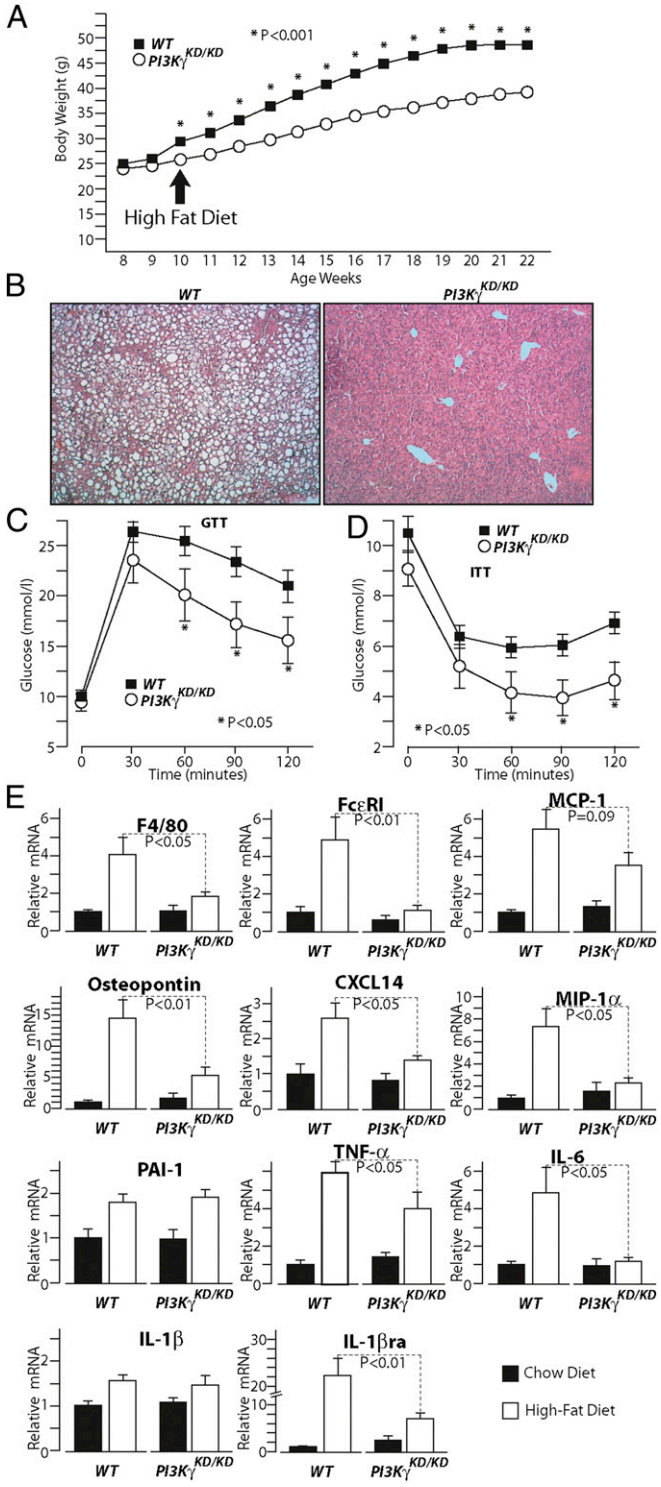

Fig. 6. Specific loss of PI3Kγ kinase-dependent signaling is sufficient to recapitulate the metabolic phenotype of *PI3Kγ*$^{-/-}$ mice. (*A*) Growth curves of WT or *PI3Kγ* kinase-dead mutants *PI3Kγ*$^{KD/KD}$ mice kept on HFD. (*B*) H&E staining of liver sections from WT or *PI3Kγ*$^{KD/KD}$ mice on HFD. (*C*) GTT of WT and *PI3Kγ*$^{KD/KD}$ mice on HFD. (*D*) ITT of WT and *PI3Kγ*$^{KD/KD}$ mice on HFD. (*E*) Real-time PCR analysis of mRNA levels of inflammatory markers in WAT from WT and *PI3Kγ*$^{KD/KD}$ mice on HFD.

diet, *PI3Kγ*$^{KD/KD}$ mice displayed similar weight gain compared with WT control mice (Fig. S7*A*) and a marginal but statistically significant improvement in glucose and insulin tolerance (Fig. S7 *B* and *C*). On HFD, *PI3Kγ*$^{KD/KD}$ mice displayed a marked reduction in weight gain (Fig. 6*A*) and were largely protected from the development of hepatic steatosis compared with WT controls (Fig. 6*B*). Glucose and insulin tolerance were also improved in *PI3Kγ*$^{KD/KD}$ mice compared with WT mice kept on HFD (Fig. 6 *C* and *D*). Consistently, WAT mRNA levels of F4/80, FcεRI, MCP-1, osteopontin, CXCL14, MIP-1α, TNF-α, IL-6, and IL-

1Ra but not PAI-1 and IL-1β were significantly reduced in $PI3K\gamma^{KD/KD}$ mice compared with WT control animals (Fig. 6*E*).

These results show that the resistance to diet-induced obesity and hepatic steatosis improved glucose homeostasis, and decreased WAT inflammation observed in $PI3K\gamma^{-/-}$ mice is largely recapitulated in $PI3K\gamma^{KD/KD}$ mice. Hence, the pathogenic action of PI3Kγ in obesity and insulin resistance depends on the lipid kinase-dependent pathway. However, these results do not exclude a possible role for PI3Kγ kinase-independent signaling in PI3Kγ-mediated metabolic modulation.

Loss of PI3Kγ Kinase-Independent Signaling Potently Induces Protein Kinase A (PKA)-Dependent, Hormone-Sensitive Lipase Phosphorylation in WAT. PI3Kγ kinase-independent signaling was shown to repress PKA-dependent phospholamban phosphorylation in cardiomyocytes (18). Given the major role of PKA in the activation of HSL and uncoupling protein 1 (UCP-1), we measured PKA-dependent HSL phosphorylation in interscapular BAT and epididimal WAT as well as UCP-1 levels in BAT. In BAT, we observed similar PKA-dependent HSL phosphorylation and UCP-1 protein levels between mice of different genotypes (Fig. 7 *A* and *B*). By contrast, in WAT, HSL phosphorylation was markedly increased at the PKA-dependent sites serine 563 and serine 660 but not at the AMPK site serine 565 in $PI3K\gamma^{-/-}$ mice but not $PI3K\gamma^{KD/KD}$ mice compared with WT controls (Fig. 7 *C* and *D*). Increased PKA-mediated HSL phosphorylation in WAT was caused by loss of PI3Kγ activity within a nonhematopoietic cell type (Fig. S5 *H* and *J*). Levels of circulating free fatty acids (FFAs) were not affected by loss of PI3Kγ activity, whereas serum leptin and insulin levels were decreased to a similar extent in $PI3K\gamma^{-/-}$ mice and $PI3K\gamma^{KD/KD}$ mice compared with WT animals (Fig. S8).

These results show that PI3Kγ kinase-independent signaling is a negative regulator of PKA-dependent HSL activation in WAT.

Discussion

Obesity is associated with a chronic low-grade inflammation (1–5), and antiinflammatory interventions may improve glycemic control in obese individuals with type 2 diabetes (6–9). Here, we describe a major role for the proinflammatory lipid kinase PI3Kγ in diet-induced obesity, fatty liver, inflammation, and insulin resistance. These results are consistent with a recent study (23) and challenge the previous idea that PI3Kγ within pancreatic β-cells is required to maintain normal glucose tolerance (20–22). The study by Kobayashi et al. (23) concluded that PI3Kγ ablation improves glucose tolerance mainly because of a direct action within leukocytes, independent from the obesity-resistant phenotype. Our data here strongly suggest that the protection from diet-induced glucose intolerance observed in $PI3K\gamma^{-/-}$ mice is mostly consequent to their leaner phenotype. We also show that diet-induced obesity, glucose intolerance, fatty liver, and metabolic inflammation depend on PI3Kγ activity within a radiation-resistant cell type of nonhematopoietic origin (Fig. 3). By contrast, PI3Kγ activity within hematopoietic cells does not affect glucose homeostasis, hepatic steatosis, and metabolic inflammation up to overtly obese mice (about 42 g) (Fig. 3). The study by Kobayashi et al. (23) reported that selective ablation of PI3Kγ activity within hematopoietic cells ameliorates glucose tolerance in morbidly obese *ob*/*ob* mice but not in mice made obese by HFD. We conclude that PI3Kγ activity within hematopoietic cells does not

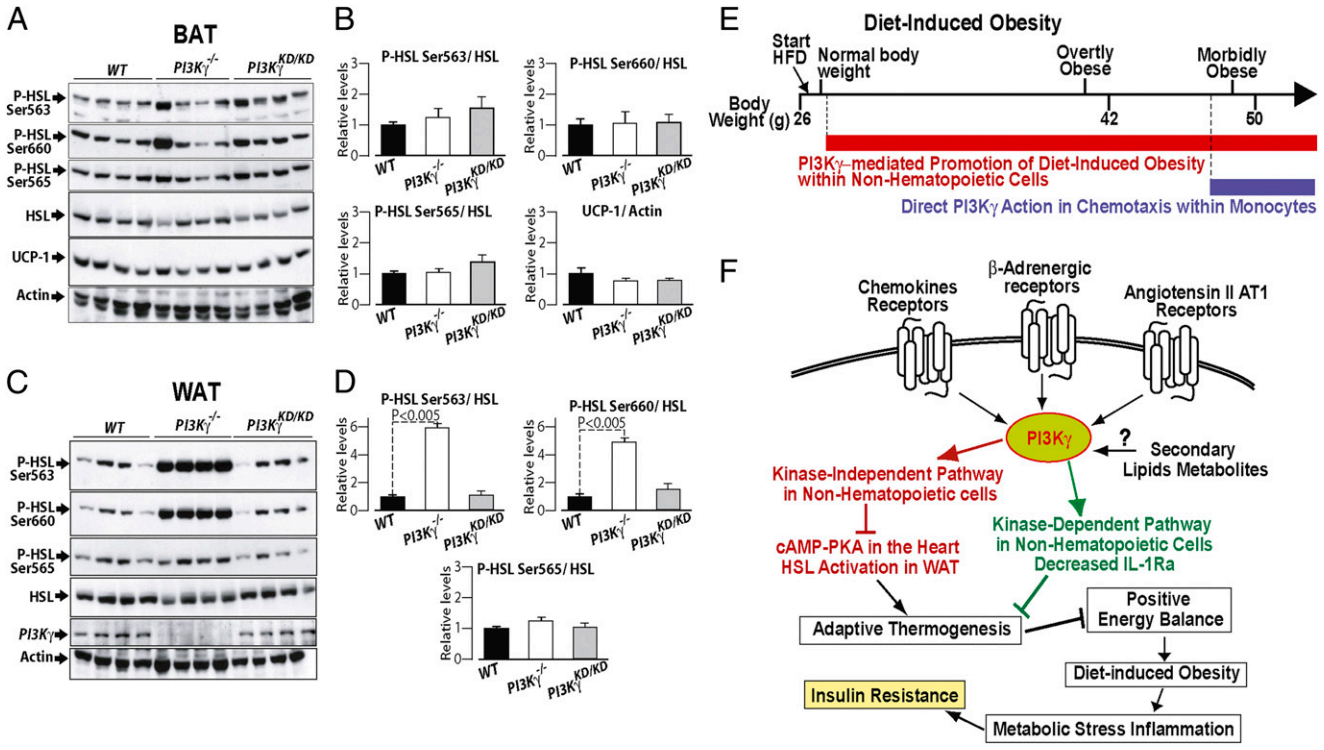

Fig. 7. PI3Kγ metabolic modulation may implicate kinase-dependent and -independent pathways. (*A*) Immunoblot analysis of HSL phosphorylation and UCP-1 protein levels in BAT extracts from WT, $PI3K\gamma^{-/-}$, and $PI3K\gamma^{KD/KD}$ mice in the fed state placed on HFD for 3 wk. (*B*) Densitometric quantification of the immunoblots in *A*. (*C*) Immunblot analysis of HSL phosphorylation in WAT. (*D*) Densitometric quantification of the immunoblots in *C*. (*E* and *F*) Our interpretation of PI3Kγ action in diet-induced obesity and insulin resistance is discussed. (*E*) PI3Kγ ablation protects from diet-induced insulin resistance by two mechanisms: (*i*) resistance to diet-induced obesity because of the lack of PI3Kγ in a nonhematopoietic compartment, which operates already from the first week of HFD and persists in time, and (*ii*) a direct effect of PI3Kγ ablation on leukocyte chemotaxis, a mechanism that is not recruited until mice reach the morbidly obese range. (*F*) Possible roles for PI3Kγ catalytic activity and kinase-independent scaffolding function in diet-induced obesity are discussed.

significantly contribute to adipose tissue inflammation and glucose intolerance until mice develop morbid obesity. Thus, at least up to overtly obese mice, promotion of diet-induced obesity within a nonhematopoietic compartment is the main pathogenic mechanism of PI3Kγ (Figs. 2 *H* and *I*, 3, and 7*E*). It is possible that a minimal threshold of PI3Kγ activity needs to be recruited to chemokine receptors within leukocytes to promote chemotaxis in vivo. Hence, PI3Kγ may contribute to leukocyte chemotaxis when levels of chemokines are sufficiently elevated, such as during infection or in morbidly obese mice (e.g., *ob*/*ob* mice), but not in normally obese mice as for most models of diet-induced obesity (Fig. 7*E*). It was reported that PI3Kγ activity in nonhematopoietic cells is required for efficient neutrophil recruitment in response to bacterial lipopolysaccharides (27). Thus, we do not exclude that PI3Kγ in nonhematopoietic cells may also play a direct role in leukocyte recruitment to the obese WAT. Nonetheless, our results show that PI3Kγ activity within nonhematopoietic cells plays a major role in energy balance in mice placed on HFD and that *PI3Kγ*$^{-/-}$ mice's leaner phenotype largely correlates with improved insulin sensitivity. The impact of PI3Kγ ablation on diet-induced obesity is striking and comparable with results typically obtained by bariatric surgery. Indeed, we typically observe a 20% reduction in body weight in *PI3Kγ*$^{-/-}$ mice compared with WT mice placed on HFD, a difference largely caused by reduced body lipids (Fig. 1). *PI3Kγ*$^{-/-}$ mice placed on HFD gained less lipid mass than WT mice, despite similar caloric intake, suggesting a decreased energetic efficiency in *PI3Kγ*$^{-/-}$ mice for lipid mass gain relative to WT animals (Fig. 4 *A*–*H*). HFD induces thermogenesis in mice by a mechanism involving β-adrenergic signaling (25, 28). Leptin was also implicated in diet-induced thermogenesis. Indeed, leptin-deficient *ob*/*ob* mice display defective thermogenic sympathetic nerve activity and dramatically impaired diet-induced thermogenesis (29–32). Interestingly, PI3Kγ is recruited to activate β-adrenergic receptors, where it plays a negative feedback (15, 18, 33, 34). Consistent with a possible role for PI3Kγ in adrenergic signaling for diet-induced thermogenesis, it was shown that PI3Kγ ablation does not protect *ob*/*ob* mice from obesity (23). We have, therefore, tested the thermogenic response to HFD feeding in WT and *PI3Kγ*$^{-/-}$ mice by calorimetry. HFD induced metabolic rate in WT and *PI3Kγ*$^{-/-}$ mice, but *PI3Kγ*$^{-/-}$ mice showed higher metabolic rate and a more pronounced thermogenic response to HFD compared with WT controls (Fig. 4 *I* and *J*). These data strongly suggest that PI3Kγ is a negative regulator of HFD-induced thermogenesis. A major factor influencing energy expenditure is adaptive thermogenesis to cold (26). Here, we show that *PI3Kγ*$^{-/-}$ mice gain significantly less weight, display improved liver steatosis and glucose tolerance, and decrease inflammation compared with WT mice kept on HFD at thermoneutrality (30 °C) (Fig. 5). However, genotypic differences were less pronounced in mice kept at thermoneutrality than in mice placed at room temperature (compare Fig. 1 with Fig. 5). We conclude that thermoregulatory thermogenesis is not an essential requirement for the metabolic phenotype of *PI3Kγ*$^{-/-}$ mice, but such phenotype may be enhanced at room temperature.

PI3Kγ signals by a kinase-dependent mechanism through PIP_3 and a kinase-independent mechanism by negative regulation of the cAMP–PKA pathway (18). Here, we show that selective inactivation of PI3Kγ kinase-dependent signaling largely recapitulates the metabolic phenotype of PI3Kγ ablation (Fig. 6). These data do not exclude a possible contribution from kinase-independent signaling but underscore the importance of the PI3Kγ kinase-dependent pathway.

β-Adrenergic signaling in BAT is considered to be essential for adaptive thermogenesis (25, 28, 35), and both cold and overfeeding induce norepinephrine turnover in the heart and BAT (36). PI3Kγ plays a negative feedback on β-adrenergic signaling in the heart, where PI3Kγ gene deletion leads to increased cAMP–PKA signaling (18). However, the role of PI3Kγ in adipose tissue is unknown. WT and *PI3Kγ*$^{-/-}$ mice displayed similar UCP-1 protein levels and HSL phosphorylation in BAT (Fig. 7 *A* and *B*). However, we observed a marked induction of PKA-dependent HSL phosphorylation (serines 563 and 660) in WAT from *PI3Kγ*$^{-/-}$ mice but not *PI3Kγ*$^{KD/KD}$ mice compared with WT controls (Fig. 7 *C* and *D*). Circulating FFAs were not affected by lack of PI3Kγ signaling (Fig. S8). Thus, HSL activation in *PI3Kγ*$^{-/-}$ adipocytes may be, per se, not sufficient to affect circulating FFA, or increased FFA release from adipocytes may be coupled to increased FFA uptake by a metabolically active cell type, possibly brown adipocytes. Overall, we have identified a role for PI3Kγ kinase-independent signaling in PKA-mediated activation of HSL in WAT. We show that PI3Kγ action on HSL activation is because of a nonhematopoietic cell type (Fig. S5 *H* and *J*). This cell may be the adipocyte itself, although it is possible that neuronal PI3Kγ may control sympathetic activity within WAT.

The molecular mechanism by which PI3Kγ promotes diet-induced obesity remains to be identified. However, we describe here PI3Kγ kinase-dependent and -independent pathways that may potentially contribute to weight gain efficiency (Fig. 7*F*). PI3Kγ is at the focal point of several signaling pathways recruited during obesity. Among the most significant are chemokine receptors, β-adrenergic receptors, and angiotensin II AT1 receptors (13–16). Consistently, mice lacking the chemokine receptor CCR2 placed on HFD display reduced body mass compared with WT mice (37), and mice lacking angiotensin II type 1A receptor or renin are resistant to diet-induced obesity because of elevated thermogenesis (38, 39). Concerning β-adrenergic signaling, where PI3Kγ plays a negative feedback, mice lacking the three forms of β-adrenergic receptors (β-less mice) develop spontaneous obesity consequent to defective adaptive thermogenesis (25, 28). On activation, PI3Kγ will negatively regulate adaptive thermogenesis by a molecular mechanism to be discovered, which operates in a nonhematopoietic compartment and may involve kinase-dependent and -independent signaling. The PI3Kγ kinase-independent pathway was shown to repress cAMP–PKA signaling in the heart (18), where sympathetic activity is elevated by overfeeding (36). Thereby, PI3Kγ kinase-independent signaling within cardiomyocytes may be implicated in diet-induced thermogensis. Here, we show that PI3Kγ kinase-independent pathway is a negative regulator of PKA-mediated HSL activation in WAT. Interestingly, PKA-induced lipolysis was shown to increase oxidative respiration in human and mouse white adipocytes (40). Concerning PI3Kγ kinase-dependent signaling, an important factor may be the imbalance in relative levels of IL-1β and IL-1Ra in mice lacking PI3Kγ activity placed on HFD. IL-1 was described as the endogenous pyrogen, because among cytokines, it is the most potent inducer of febrile thermogenesis (41). Strong evidence supporting the idea that a reduced IL-1Ra/IL-1β ratio may contribute to decreased metabolic efficiency in *PI3Kγ*$^{-/-}$ mice came from mouse genetics studies. Mice lacking IL-1 type I receptor develop mature-onset obesity on standard diet (42). Consistently, mice that do not express IL-1Ra are resistant to diet-induced obesity because of increased metabolic rate (43). Furthermore, it was shown that the thermogenic effects of central leptin signaling are blocked by injection of IL-1Ra (44). Hence, whereas acute pharmacological administration of IL1-Ra improves glucose homeostasis in diabetics (8), a large body of evidence indicates that chronically elevated IL-1Ra relative to lower IL-1β promotes obesity through suppression of adaptive thermogenesis (42–45). Here, we show that expression of IL-1Ra, but not IL-1β, in obese WAT is markedly reduced in *PI3Kγ*$^{-/-}$ and *PI3Kγ*$^{KD/KD}$ mice compared with WT animals made obese by HFD. Thus, reduced IL-1Ra expression may contribute to the PI3Kγ kinase-dependent effects on energetic efficiency for fat mass gain.

Our results, together with the results from the study by Kobayashi et al. (23) and previous reports on PI3Kγ in models of

atherosclerosis (46, 47) and angiotensin II-mediated vasculotoxic and hypertensive effects (16), strongly suggest that PI3Kγ should be regarded as a most valuable drug target for the treatment of obesity-related diseases. Our data also suggest that a most effective drug targeting this pathway should efficiently inhibit PI3Kγ within the nonhematopoietic compartment responsible for the leaner phenotype of *PI3Kγ*$^{-/-}$ mice.

Experimental Procedures

Experimental Models. Mice were males on C57BL6/J background. *PI3Kγ*$^{-/-}$ and *PI3Kγ*$^{KD/KD}$ mice were previously described (13, 18). HFD (60% of calories from fat) was purchased from Bio-Serv (diet F3282). Mice were kept at our standard facility under 12-h light and 12-h dark cycles at room temperature (23 °C) except for the thermoneutrality experiment, where mice were kept in an incubator at 30 °C. Radiation chimeras were generated essentially as previously described (24) using congenic donors and recipients that differed at the Ly5.1/Ly5.2 locus. Briefly, recipient mice received the lethal dose of 950 Rad of ionizing radiation followed by tail vein injection of 10^7 bone marrow cells. Mice were maintained on chow diet for 6 wk to allow bone marrow reconstitution; the first 5 wk included antibiotics (polymyxin, 13 mg/L; neomycin, 25 mg/L). After reconstitution, mice were placed on HFD for 20 wk. Experimental procedures were authorized by the cantonal veterinary committees.

Flow Cytometry. Reconstitution efficiency was evaluated by flow cytometry analysis for Ly5.1 (D45.1) and Ly5.2 (CD45.2). Whole blood was collected and stained with anti-CD45.2–FITC and anti-CD45.1–PE-Cy7 together with antibodies against T cells or macrophage markers (CD3-PE or CD11b-PerPc Cy5.5). For evaluation of mast cell reconstitution, peritoneal cells were collected by PBS lavage and stained with anti-CD45.2–FITC and anti-CD45.1–PE-Cy7 together with antibodies against FcεRI-PE and cKit-APC. Cells were washed, resuspended in FACS buffer, and analyzed by FACSCanto-II (BD Biosciences). Data were plotted using FlowJo software.

Energy Balance. For precise food intake measurement, HFD was placed in glass beakers (2-cm diameter) fixed on the cage wall to avoid spillage. Analysis of fecal lipid content was performed by gravimetric analysis of dry chloroform–methanol extracts as previously described (48). Body composition analysis was performed on carcasses as previously described (49). Body water was calculated as the difference between total body weight and dry weight after desiccation in the oven at 75 °C until constant weight. Lipid-free dry mass was measured by gravimetric analysis of the homogenized dry carcasses after Soxhlet lipid extraction. Lipid mass was calculated as the difference between dry mass and lipid-free dry mass. Indirect calorimetry analysis and simultaneous physical activity measurement were performed using the Oxymax Comprehensive Lab Animal Monitoring System (Columbus Instruments). Mice were placed in the calorimeter for 3 d on chow diet and then switched to HFD for 3 more d; the first 2 d of chow diet are used as the acclimation period, and data are collected from the third day of chow diet. The calorimetry study is designed to have no statistically significant difference in body weight and composition between WT mice and *PI3Kγ*$^{-/-}$ mice when we started the analysis to simplify data interpretation (50).

Glucose Homeostasis and Insulin Sensitivity. Mice were fasted 6 h before GTT or ITT test. For GTT, mice were injected i.p. with a glucose bolus of 1 g/kg body weight, whereas for ITT, mice were injected i.p. with either 1 iU insulin/kg body weight for the HFD groups or 0.75 iU/kg body weight for the chow diet and radiation chimeras groups. For hyperinsulinemic euglycemic clamp, an indwelling catheter for insulin and glucose infusion was placed into the left femoral vein under anesthesia. Mice were allowed to recover for 6–8 d until they regained 95–100% of initial body weight. After a 5-h fast, a 180-min hyperinsulinemic euglycemic clamp study was conducted in awake, freely moving mice as previously described (51, 52). Briefly, [3-^{3}H]-glucose (NEN Life Sciences) was prime-infused throughout the clamp [10 μCi bolus followed by 0.05 μCi/min (basal) and 0.1 μCi/min (clamp)] to estimate glucose turnover and hepatic glucose production. After an 80-min basal period, a blood sample was collected for determination of basal glucose turnover. The clamp was initiated by prime infusion of human insulin (Actrapid; Novo Nordisk) at 6 mU/kg per min, and 30% glucose was infused at rates to clamp plasma glucose levels around 8.4 mM. After 2 h, a bolus (10 μCi) of 2-deoxy-D-[1-^{14}C]-glucose (2-[^{14}C]DOG) (NEN Life Sciences) was injected. At the end of the clamp study, mice were killed, and tissues were collected for subsequent analysis. Plasma samples were analyzed for glucose concentration and [^{3}H] glucose and 2-[^{14}C]DOG concentrations. For the determination of 2-[^{14}C] DOG tissue uptake, tissue samples were homogenized, and the supernatants were passed through ion exchange columns to separate 2-[^{14}C]DOG-6-phosphate from 2-[^{14}C]DOG.

Molecular Measurements and Adipocytes Size. Total RNA was isolated from tissues by guanidinium–thiocyanate extraction. cDNA was prepared using a reverse transcription kit (Promega), and qPCR was performed using a commercial SYBR green mix (Applied Biosystems) using specific primers (Table S1). Ex vivo insulin signaling on extensor digitorum longus muscles was performed as described (53) using a submaximal stimulatory dose of insulin (0.1 μM). Stromal vascular and adipocytes fractions where prepared by collagenase digestion (Roche) of WAT to obtain a single cell suspension, which was separated into stromal vascular fractions and mature adipocytes by centrifugation. For immunoblot analysis, PI3Kγ polyclonal antibodies were previously described (54), and other commercial antibodies were antitubulin and antiactin (Sigma), UCP-1 (Alpha Diagnostic International), total AKT and AKT serine 473, total HSL, and phospho-specific antibodies for serines 563, 660, and 595 of HSL (Cell Signaling). Quantification of adipose tissue crown-like structures was performed as previously described (24, 55). Adipocytes size distributions analysis was performed by computer image analysis of tissue sections as described (56).

Statistical Analysis. Data are shown as means, and error bars indicate SEs. We performed two-way ANOVA for the GTT and ITT data expressed as percent variation from baseline, whereas for all other data, *P* values where calculated by Student *t* test. $P < 0.05$ is considered statistically significant.

ACKNOWLEDGMENTS. We thank Katrin Hafen for valuable technical assistance with the chimera generation. This study is supported by a Novartis Research Foundation Fellowship (to B.B.), Swiss National Science Foundation Grants 310030-127574 (to M.P.W.), 31EM30-126143 (to M.P.W.), 31003A-118172 (to G.S.), and 31003A_135684 (to G.S.), and the European Foundation for the Study of Diabetes (EFSD)/Lilly Fellowship Award and the EFSD Diabetes and Cancer Grant (to G.S.).

1. Shoelson SE, Lee J, Goldfine AB (2006) Inflammation and insulin resistance. *J Clin Invest* 116:1793–1801.
2. Hotamisligil GS (2006) Inflammation and metabolic disorders. *Nature* 444:860–867.
3. Schenk S, Saberi M, Olefsky JM (2008) Insulin sensitivity: Modulation by nutrients and inflammation. *J Clin Invest* 118:2992–3002.
4. Lumeng CN, Maillard I, Saltiel AR (2009) T-ing up inflammation in fat. *Nat Med* 15: 846–847.
5. Solinas G, Karin M (2010) JNK1 and IKKbeta: Molecular links between obesity and metabolic dysfunction. *FASEB J* 24:2596–2611.
6. Reid J, MacDougall AI, Andrews MM (1957) Aspirin and diabetes mellitus. *BMJ* 2: 1071–1074.
7. Yazdani-Biuki B, et al. (2004) Improvement of insulin sensitivity in insulin resistant subjects during prolonged treatment with the anti-TNF-alpha antibody infliximab. *Eur J Clin Invest* 34:641–642.
8. Larsen CM, et al. (2007) Interleukin-1-receptor antagonist in type 2 diabetes mellitus. *N Engl J Med* 356:1517–1526.
9. Fleischman A, Shoelson SE, Bernier R, Goldfine AB (2008) Salsalate improves glycemia and inflammatory parameters in obese young adults. *Diabetes Care* 31:289–294.
10. Jia S, et al. (2008) Essential roles of PI(3)K-p110beta in cell growth, metabolism and tumorigenesis. *Nature* 454:776–779.
11. Ciraolo E, et al. (2008) Phosphoinositide 3-kinase p110beta activity: Key role in metabolism and mammary gland cancer but not development. *Sci Signal*, 10.1126/scisignal.1161577.
12. Foukas LC, et al. (2006) Critical role for the p110alpha phosphoinositide-3-OH kinase in growth and metabolic regulation. *Nature* 441:366–370.
13. Hirsch E, et al. (2000) Central role for G protein-coupled phosphoinositide 3-kinase gamma in inflammation. *Science* 287:1049–1053.
14. Quignard JF, et al. (2001) Phosphoinositide 3-kinase gamma mediates angiotensin II-induced stimulation of L-type calcium channels in vascular myocytes. *J Biol Chem* 276: 32545–32551.
15. Naga Prasad SV, Barak LS, Rapacciuolo A, Caron MG, Rockman HA (2001) Agonist-dependent recruitment of phosphoinositide 3-kinase to the membrane by beta-adrenergic receptor kinase 1. A role in receptor sequestration. *J Biol Chem* 276:18953–18959.
16. Vecchione C, et al. (2005) Protection from angiotensin II-mediated vasculotoxic and hypertensive response in mice lacking PI3Kgamma. *J Exp Med* 201:1217–1228.
17. Wymann MP, et al. (2003) Phosphoinositide 3-kinase gamma: A key modulator in inflammation and allergy. *Biochem Soc Trans* 31:275–280.
18. Patrucco E, et al. (2004) PI3Kgamma modulates the cardiac response to chronic pressure overload by distinct kinase-dependent and -independent effects. *Cell* 118: 375–387.

19. Bohnacker T, et al. (2009) PI3Kgamma adaptor subunits define coupling to degranulation and cell motility by distinct PtdIns(3,4,5)P3 pools in mast cells. *Sci Signal*, 10.1126/scisignal.2000259.
20. MacDonald PE, et al. (2004) Impaired glucose-stimulated insulin secretion, enhanced intraperitoneal insulin tolerance, and increased beta-cell mass in mice lacking the p110gamma isoform of phosphoinositide 3-kinase. *Endocrinology* 145:4078–4083.
21. Li LX, et al. (2006) Role of phosphatidylinositol 3-kinasegamma in the beta-cell: Interactions with glucagon-like peptide-1. *Endocrinology* 147:3318–3325.
22. Pigeau GM, et al. (2009) Insulin granule recruitment and exocytosis is dependent on p110gamma in insulinoma and human beta-cells. *Diabetes* 58:2084–2092.
23. Kobayashi N, et al. (2011) Blockade of class IB phosphoinositide-3 kinase ameliorates obesity-induced inflammation and insulin resistance. *Proc Natl Acad Sci USA* 108: 5753–5758.
24. Solinas G, et al. (2007) JNK1 in hematopoietically derived cells contributes to diet-induced inflammation and insulin resistance without affecting obesity. *Cell Metab* 6: 386–397.
25. Bachman ES, et al. (2002) betaAR signaling required for diet-induced thermogenesis and obesity resistance. *Science* 297:843–845.
26. Stock MJ (1999) Gluttony and thermogenesis revisited. *Int J Obes Relat Metab Disord* 23:1105–1117.
27. Puri KD, et al. (2005) The role of endothelial PI3Kgamma activity in neutrophil trafficking. *Blood* 106:150–157.
28. Jimenez M, et al. (2002) Beta(1)/beta(2)/beta(3)-adrenoceptor knockout mice are obese and cold-sensitive but have normal lipolytic responses to fasting. *FEBS Lett* 530: 37–40.
29. Trayhurn P, Jones PM, McGuckin MM, Goodbody AE (1982) Effects of overfeeding on energy balance and brown fat thermogenesis in obese (ob/ob) mice. *Nature* 295: 323–325.
30. Mistry AM, Swick AG, Romsos DR (1997) Leptin rapidly lowers food intake and elevates metabolic rates in lean and ob/ob mice. *J Nutr* 127:2065–2072.
31. Young JB, Landsberg L (1983) Diminished sympathetic nervous system activity in genetically obese (ob/ob) mouse. *Am J Physiol* 245:E148–E154.
32. Haynes WG, Sivitz WI, Morgan DA, Walsh SA, Mark AL (1997) Sympathetic and cardiorenal actions of leptin. *Hypertension* 30:619–623.
33. Naga Prasad SV, et al. (2002) Phosphoinositide 3-kinase regulates beta2-adrenergic receptor endocytosis by AP-2 recruitment to the receptor/beta-arrestin complex. *J Cell Biol* 158:563–575.
34. Naga Prasad SV, Jayatilleke A, Madamanchi A, Rockman HA (2005) Protein kinase activity of phosphoinositide 3-kinase regulates beta-adrenergic receptor endocytosis. *Nat Cell Biol* 7:785–796.
35. Rothwell NJ, Stock MJ (1979) A role for brown adipose tissue in diet-induced thermogenesis. *Nature* 281:31–35.
36. Landsberg L, Saville ME, Young JB (1984) Sympathoadrenal system and regulation of thermogenesis. *Am J Physiol* 247:E181–E189.
37. Weisberg SP, et al. (2006) CCR2 modulates inflammatory and metabolic effects of high-fat feeding. *J Clin Invest* 116:115–124.
38. Kouyama R, et al. (2005) Attenuation of diet-induced weight gain and adiposity through increased energy expenditure in mice lacking angiotensin II type 1a receptor. *Endocrinology* 146:3481–3489.
39. Takahashi N, et al. (2007) Increased energy expenditure, dietary fat wasting, and resistance to diet-induced obesity in mice lacking renin. *Cell Metab* 6:506–512.
40. Yehuda-Shnaidman E, Buehrer B, Pi J, Kumar N, Collins S (2010) Acute stimulation of white adipocyte respiration by PKA-induced lipolysis. *Diabetes* 59:2474–2483.
41. Dinarello CA (2010) IL-1: Discoveries, controversies and future directions. *Eur J Immunol* 40:599–606.
42. García MC, et al. (2006) Mature-onset obesity in interleukin-1 receptor I knockout mice. *Diabetes* 55:1205–1213.
43. Somm E, et al. (2005) Decreased fat mass in interleukin-1 receptor antagonist-deficient mice: Impact on adipogenesis, food intake, and energy expenditure. *Diabetes* 54:3503–3509.
44. Luheshi GN, Gardner JD, Rushforth DA, Loudon AS, Rothwell NJ (1999) Leptin actions on food intake and body temperature are mediated by IL-1. *Proc Natl Acad Sci USA* 96:7047–7052.
45. Juge-Aubry CE, et al. (2003) Adipose tissue is a major source of interleukin-1 receptor antagonist: Upregulation in obesity and inflammation. *Diabetes* 52:1104–1110.
46. Chang JD, et al. (2007) Deletion of the phosphoinositide 3-kinase p110gamma gene attenuates murine atherosclerosis. *Proc Natl Acad Sci USA* 104:8077–8082.
47. Fougerat A, et al. (2008) Genetic and pharmacological targeting of phosphoinositide 3-kinase-gamma reduces atherosclerosis and favors plaque stability by modulating inflammatory processes. *Circulation* 117:1310–1317.
48. Folch J, Lees M, Sloane Stanley GH (1957) A simple method for the isolation and purification of total lipides from animal tissues. *J Biol Chem* 226:497–509.
49. Summermatter S, et al. (2009) Adipose tissue plasticity during catch-up fat driven by thrifty metabolism: Relevance for muscle-adipose glucose redistribution during catch-up growth. *Diabetes* 58:2228–2237.
50. Butler AA, Kozak LP (2010) A recurring problem with the analysis of energy expenditure in genetic models expressing lean and obese phenotypes. *Diabetes* 59: 323–329.
51. Preitner F, Mody N, Graham TE, Peroni OD, Kahn BB (2009) Long-term Fenretinide treatment prevents high-fat diet-induced obesity, insulin resistance, and hepatic steatosis. *Am J Physiol Endocrinol Metab* 297:E1420–E1429.
52. Minehira K, et al. (2008) Blocking VLDL secretion causes hepatic steatosis but does not affect peripheral lipid stores or insulin sensitivity in mice. *J Lipid Res* 49:2038–2044.
53. Solinas G, et al. (2004) The direct effect of leptin on skeletal muscle thermogenesis is mediated by substrate cycling between de novo lipogenesis and lipid oxidation. *FEBS Lett* 577:539–544.
54. Bondeva T, et al. (1998) Bifurcation of lipid and protein kinase signals of PI3Kgamma to the protein kinases PKB and MAPK. *Science* 282:293–296.
55. Cinti S, et al. (2005) Adipocyte death defines macrophage localization and function in adipose tissue of obese mice and humans. *J Lipid Res* 46:2347–2355.
56. Chen HC, Farese RV, Jr. (2002) Determination of adipocyte size by computer image analysis. *J Lipid Res* 43:986–989.